



The October 29, 2018 storm in Northern Italy – An exceptional event and its modeling



L. Cavaleri^{a,*}, M. Bajo^a, F. Barbariol^a, M. Bastianini^a, A. Benetazzo^a, L. Bertotti^a, J. Chiggiato^a, S. Davolio^b, C. Ferrarin^a, L. Magnusson^c, A. Papa^d, P. Pezzutto^a, A. Pomaro^a, G. Umgiesser^a

^a CNR-ISMAR, Venice, Italy

^b ISAC, Bologna, Italy

^c ECMWF, Reading, UK

^d CPSM, Venice, Italy

ARTICLE INFO

Keywords:

Storm
Extreme conditions
Cyclogenesis
Wind waves
Coastal processes
Storm surge

ABSTRACT

On October 29, 2018 a very severe storm affected Northern Italy, including the Adriatic Sea. The ensuing surge and wave conditions at and in front of Venice stand at the extreme tail of the respective historical return period distributions. The large set of available measured data, at the coast and at the offshore oceanographic tower, coupled with detailed numerical simulations, allows a keen analysis of the storm, its predictability and in particular of the ensuing enhanced coastal processes. These include the coastal set-up, the input information for tidal prediction in Venice, the documented passage of an atmospheric cold front and, using the local tidal data, the derived possibility of estimating the surface wind stress, the evidence of reflected waves from the coast and the associated seismometers signal 40 km inland. The highest crest and wave heights measured at the tower are beyond what is suggested by non-linear statistics. The relative out-of-scale magnitude of the three major storms since 1966 suggests the possibility that they belong to a self-standing family of events.

1. Introduction

The storm we consider in this paper developed at the end of October in the Western Mediterranean Sea as an explosive cyclogenesis following a cold input from the Gulf of Lion (see Fig. 1 for the geographical references). Born West of Sardinia, the ensuing very compact low deepened rapidly moving at high speed toward North. The low forced strong winds on its right flank that led to destructive (compared to the local standards) waves in the Ligurian Sea. At the same time the low led also to a very strong South-East sirocco wind in the Adriatic Sea, with consequent high waves in front of Venice and a substantial surge that only by a lucky coincidence did not occur to be by far the worst in documented history. In this paper we analyze the storm (generally known as Vaia), focusing our attention on the Adriatic events. The evolution of the storm, located on the tail of the related historical extremal distribution, led to peculiar conditions in front of Venice, conditions that, thanks to the extensive measurements available

at the coast and at the CNR-ISMAR (henceforth ISMAR) oceanographic tower (15 km offshore), pushed us to further investigate the mechanisms of coastal processes. The abundance of data and the extensive modeling allow discussing in sequence several different aspects of the storm. With this background the paper is organized as follows.

Section 2 provides a comprehensive, although compact, description of the meteorology of the storm and of what was peculiar in its various severe aspects. Focusing mainly on the Adriatic Sea, Section 3 lists the available measured data, both from the local sources and by remote sensing. The general modeling approach, covering meteorology and oceanography, the latter both for waves and surge (implicitly circulation), is given in Section 4. In Section 5 we report and discuss the corresponding model results. Being the heart of the paper, this section is more comprehensive than the other sections, examining the details of the basic cited parameters, i.e., wind, waves and surge. The non-negligible aspect of predictability is dealt with in Section 6, leading also to an interesting comparison with the two similar storms of 1966 and

Abbreviations: ADCP, Acoustic Doppler Current Profiler; CNR-ISMAR, Consiglio Nazionale delle Ricerche – Istituto di Scienze Marine; CPSM, Centro Previsione e Segnalazione Maree; ECWAM, ECMWF WAM model; ECMWF, European Centre for Medium-Range Weather Forecasts; HRES, High Resolution; IBI, Iberia–Biscay–Ireland; SHYFEM, Shallow water HYdrodynamic Finite Element Model; UKMO, United Kingdom Meteorological Office; UTC, Universal Time Coordinate; WAM, WAve Model

* Corresponding author at: ISMAR, Arsenale – Tesa 104, Castello 2737/F, 30122 Venice, Italy.

E-mail address: luigi.cavaleri@ismar.cnr.it (L. Cavaleri).

<https://doi.org/10.1016/j.pocean.2019.102178>

Received 25 March 2019; Received in revised form 18 July 2019; Accepted 25 August 2019

Available online 26 August 2019

0079-6611/ © 2019 Elsevier Ltd. All rights reserved.



Fig. 1. Western and central Mediterranean Sea. The main geographical features and the relevant locations are indicated. The lines show respectively: (A) the path and timing of the cyclogenesis minimum, (B) the direction of the strong winds associated with it, (C) the direction of the sirocco winds on the Adriatic Sea, (D) the path followed by the violent cold front. The small rectangle on Venice indicates the area enlarged in Fig. 3.

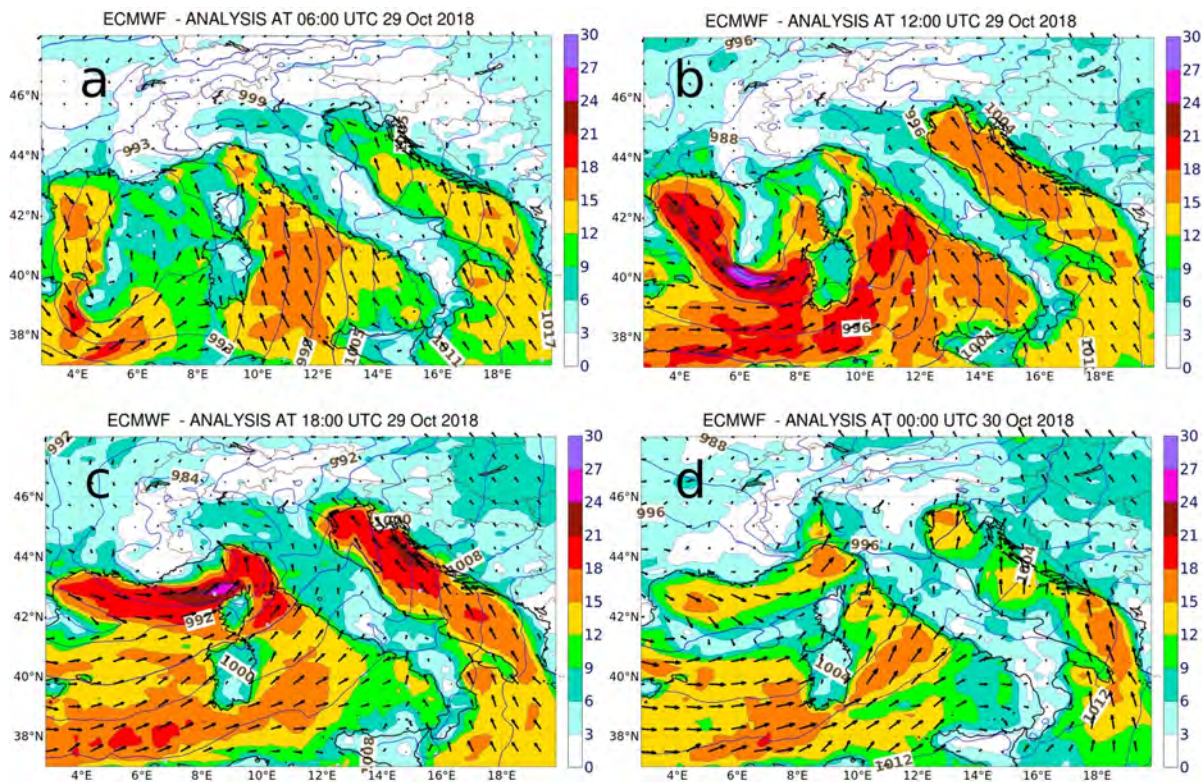


Fig. 2. Surface wind speed (ms^{-1}) and surface pressure fields on the Western Mediterranean Sea. The four panels show the ECMWF analysis at respectively (UTC time of 29 and 30 October 2018): (a) 06–29, (b) 12–29, (c) 18–29, (d) 00–30.

1979. In [Section 7](#) we delve into the physics of coastal hydrodynamic processes taking advantage of the availability of data at the coast and at the tower position, 15 km offshore. In [Section 8](#) we focus on the conditions at the tower and attempt to relate the possible extremes derived from the wave model spectra with the ones available from direct records and deduced from the damages on some light-structures of the tower. The statistical significance of the storm is assessed in [Section 9](#) as derived from the long-term locally available records. All this is critically discussed in [Section 10](#) where we point out the successes, but, most of all, the small and not so small errors of the models, deriving, or at least discussing, where problems may lie and improvements are required. All this is itemized in the final [Section 11](#). A dedicated list explains the meaning of the various acronyms.

2. The meteorological evolution of the storm

In late October 2018 the synoptic characteristics of the weather conditions over the Western Mediterranean Sea resembled the typical pattern associated with major rain events over the southern side of the Alpine range. A large-scale cyclonic system was slowly evolving, leading to southerly flow towards the Alps (see [Fig. 1](#) for the geography of the area), with consequent intense alpine precipitation events. At the surface the wind over the sea was oriented from South-East in the form of a low level jet over both the Tyrrhenian and Adriatic seas, respectively to the West and East of Italy. After a short lull, a second and more intense phase of the event took place on the 29th, when a cold front from the Gulf of Lion entered the Mediterranean basin (panel 2a, at 06 UTC). The interaction between the cold inflow with the warm and moist marine boundary layer triggered the rapid intensification of the low that, starting from the general field, quickly underwent (12 UTC, panel 2b) an explosive cyclogenesis with central pressure estimated at 984 hPa. The cyclone moved rapidly northward (A in [Fig. 1](#); note timing of its sequential positions) while still deepening down to 977 hPa (U.K. Meteorological Office) and further reducing its horizontal scale. Moving North, the low forced strong south-easterly winds on its right flank, both on the Tyrrhenian Sea (B in [Fig. 2](#), with the flow squeezed between the low and the Apennines range along the peninsula) and the Adriatic Sea (C, here enhanced by the high pressure over eastern Europe). The winds led to high waves both on the Ligurian Sea and the Northern Adriatic Sea. The low entered land north of Corsica at about 18 UTC, followed (D) by a strong and violent flow of cold air from West-South-West (panel 2c, 18 UTC). This very energetic cold flow quickly passed over the Apennines, precipitating into the Adriatic basin. In a way this halted the flood of Venice, but, forcing the sirocco wind into a narrower path against the Eastern Alps, it also led to tremendously strong winds in the mountain area (Dolomites and Eastern Alps), with record wind speeds (gusts up to 213 kmh^{-1} recorded before the instrument failed) and very extensive forest damage (estimated loss of 11 million trees). On the Adriatic Sea, where we focus our attention, the wind was over at 00 UTC of the 30th (panel 2d), while of course the long swell was still pounding on the Venetian coast.

3. The observational dataset

[Fig. 3](#) provides the geometry of the Venetian coast (area marked in [Fig. 1](#)) and a view of the ISMAR oceanographic tower “Acqua Alta” (literally “high water”, a superstitious name following its construction after the big flood of 1966 – [Trincardi et al., 2016](#), provide a full description of the event). [Cavaleri \(2000\)](#) provides an extensive description of the original tower structure, now further improved and 2 m higher, the measurements on board and the derived scientific work. 15 km offshore and with the template (basic holding structure) firmly implanted on the 16 m bottom, the above four working decks are now (after the recent renovation works and structural extension) respectively at 6.5, 9, 12 and 15 m above the mean sea level (1, 2, 3, 4 in [Fig. 3](#)). Both data and minor damage on the horizontal outgoing

platform (deck 2) provide evidence of up to +9 m crest heights (but with +1.30 m surge). In these respects the storm was a repetition of the 22 December 1979 event (flood ranked #2 in Venice) for which no data, except the evidence from damage, are available. Most of the on-board instruments are managed by ISMAR, but the tower also hosts instruments by other institutions, in particular CPSM (the tidal forecast center of the Municipality of Venice) and Thetis, a local environmental enterprise.

The data collected at the tower include the following relevant parameters for our present purposes:

Winds – two anemometers (ISMAR and CPSM) at 20 and 18 m height, respectively, 5 and 3 m above the tower upper deck. Data (mean wind speed, gust, direction) are available at 5-min interval.

Waves – Five different wave systems are operated on board: (a) AWAC (Nortek AS) located at 16 m depth, 20 m east of the tower (ISMAR). The system is composed of an acoustic doppler current meter (which can also work as a profiler), an acoustic surface tracker and a pressure sensor. Integral parameters are available in real time, usually estimated from the current meter and the surface tracker. The monthly retrieved raw data, then suitably analyzed, offer the possibility of 1D and 2D spectral estimates. The pressure sensor provides parallel wave measurements, potentially less accurate, but used when the many bubbles in water, following heavy wave breaking in a storm, impede a clean acoustic signal. The current meter and pressure sensor are set to operate at 2 Hz, while the surface tracker samples the water level at 4 Hz. (b) A radar surface profiler (Thetis) sampling at 2 Hz. Integral parameters are available in real time, 1D spectra after the raw data recovery. (c) An external acoustic echo-sounder (CPSM) sampling the surface at 2 Hz. Only integral parameters (no raw data) are available. The gauge worked until a wave (possibly a splash) hit and damaged it. Regardless of this, problems seem to appear in strong wind conditions. (d) A stereo-imaging system (ISMAR) observing to the Northeast direction the area close to the tower (the waves were from South-East). The system, usable only with the daylight, provides a very detailed 2D spectrum of the wavy surface (see [Peureux et al., 2018](#); [Benetazzo et al., 2018](#)). (e) Webcams showing, apart from incoming waves, one of the pillars of the tower with direct evidence of the vertical excursion of the sea surface. Both the stereo system and the webcam signals are remotely recorded and stored for later inspection and analysis. The optical flow of information, in any case available only during the daylight, stopped around 14 UTC because of power failure in the Venice area where is the receiver.

Sea level – Four instruments: (a) A conventional tide gauge (CPSM) with data at 5-min interval. (b) A similar system handled by ISMAR. (c) A digitally filtered radar system by Thetis. (d) The ISMAR ADCP.

On the coast and the lagoon (see [Fig. 3](#), left panel) tidal data (CPSM) are available at the end of the Lido entrance jetties (2 km offshore, 6 m depth), at Malamocco and Chioggia inlets, and at several locations in the lagoon, including Punta Salute (the dot close to Venice), the official reference for Venice floods. All these instruments are of the standard tidal well type with a float, with digital recording.

4. Wind, wave and surge modeling

We deal with the meteorological, wave and surge aspects of the storm, the last two ones focused on the Adriatic Sea. We describe briefly the models used. For a better understanding of the storm impacts, we provide a short description of the local dominant characteristics and weather patterns.

4.1. Characterization of the area

The Adriatic Sea (see [Fig. 1](#) and [Fig. 4](#)) is a long and narrow basin bordered by mountains on both sides. It is characterized, especially in its northerly section, by two dominant winds: bora and sirocco. Bora, blowing from North-East (henceforth, given their frequent use, we will

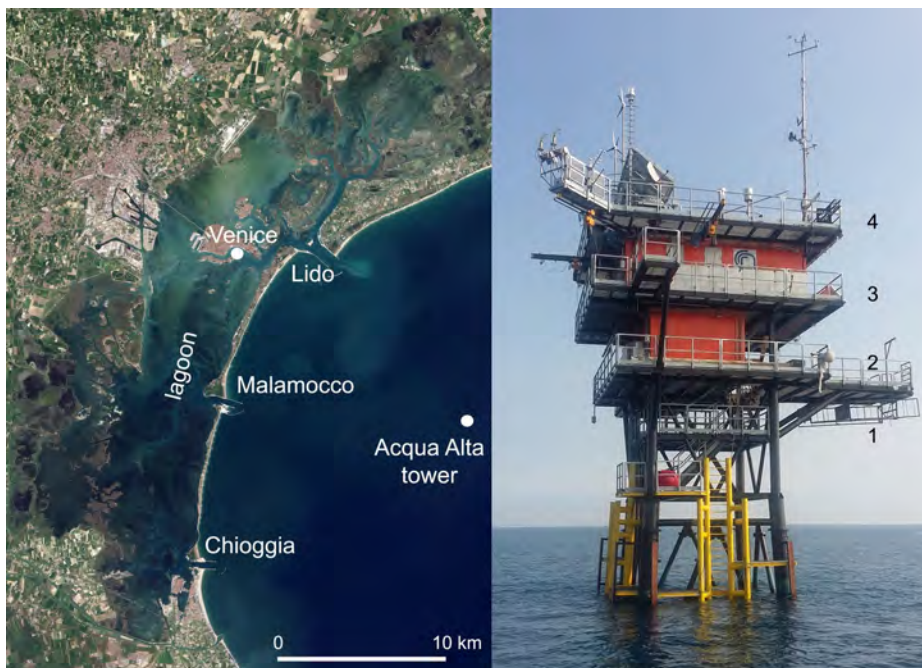


Fig. 3. Left panel: geometry of the area at the top of the Adriatic Sea (see Fig. 1). The ‘tower’ is the position of the offshore structure shown in the right panel. Lido, Malamocco and Chioggia are the three inlets connecting the sea with the lagoon. The Venice dot shows Punta Salute, the official tide gauge for Venice floods. 1, 2, 3, 4 (in the right panel) identify the four usable decks of the tower, at respectively 6.5, 9, 12, 15 m above the mean sea level.

indicate the four cardinal points as N-E-S-W, with obvious meaning), can be very strong (up to 30 ms^{-1}), but, because of fetch limitations, the derived wave conditions are not very large. The opposite is true for sirocco, the S-E wind typically responsible for the Venice floods. Warmer and humid, it is often associated to a low pressure center on the Western Mediterranean basin. Sometimes, also blocked by the Alps range (see Fig. 1), in the northern part of the basin the wind mixes with easterly air leading to the so called “bora scura”, because of the associated cloudy and rainy conditions.

The astronomical tide in the Northern Adriatic Sea, in front of Venice (see Fig. 3), has about one meter spring overall excursion. When the basin is perturbed by a meteorological event, two seiches dominate the situation: an 11-h one rocking about the basin center, and a 22 h one with the node at the Otranto strait, at the southern end of the basin (Bajo et al., 2019). The bathymetry is progressively shallower towards the Venice upper end (see Fig. 1). Together with the dominant weather patterns, this leads to frequent and comparably large surges on its northern border, i.e. in front of Venice. See Fig. 4, panel c, for a clear illustration of this distribution. As shown in Fig. 3, Venice sits at the center of a coastal, $50 \times 10 \text{ km}$ wide, mostly shallow lagoon connected to the sea via three inlets.

When referring to the last days of October 2018, only the day (e.g., 29 for 29 October 2018) will be specified. Not mentioning the day will

imply that what discussed is on 29 (when in practice everything happened). For time, all UTC, e.g. 19.10 UTC will mean 10 min after 19 UTC.

4.2. Meteorology

In this study we rely on the meteorological data produced by the European Centre for Medium-Range Weather Forecasts operational model (ECMWF, Reading, U.K.). The Centre runs a fully coupled atmosphere-wave-ocean system. Presently the Tco1279 (HRES) atmospheric model (see the full documentation available at <https://www.ecmwf.int/en/forecasts/documentation-and-support/changes-ecmwf-model/ifs-documentation>) has approximately 9-km resolution and 137 vertical levels 20 of which are below 1000 m. Ensemble forecasts are also produced with 50 parallel runs at 18-km resolution. The operational analyses are based on 4-dimensional variational data assimilation (Rabier et al., 2007). The analysis data are available at 6 h intervals (00, 06, 12, 18 UTC). This time resolution is unsuitable for our purpose (in practice everything happened in 12 h), thus we are concatenating the first 12-h short-term forecast fields, available at one hour interval twice a day at 00 and 12 UTC. To explore its predictability, we have used the medium-range forecast for the 29 October starting up to ten days earlier for HRES, fifteen for the ensemble. Although our evaluation is based on

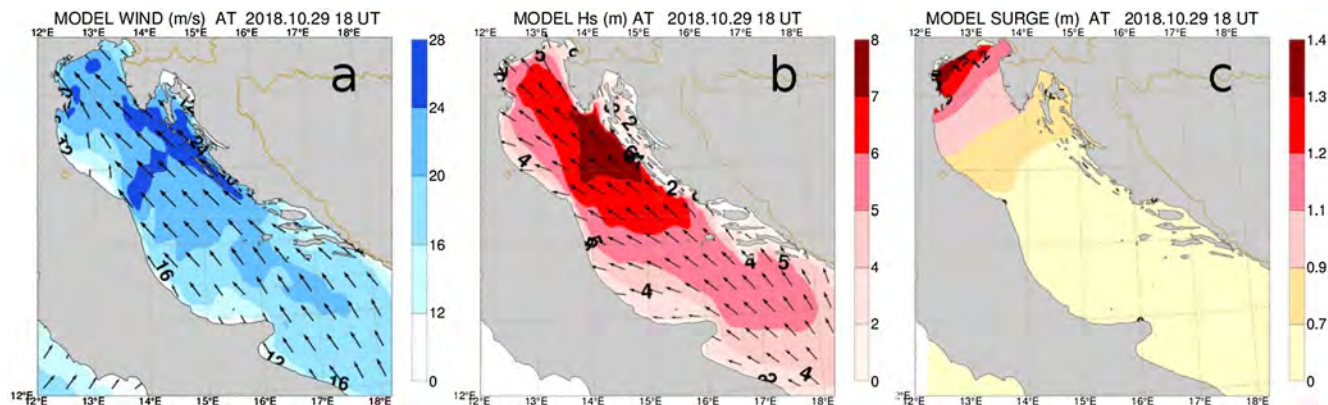


Fig. 4. (a) Wind, (b) wave, (c) surge fields in the Adriatic Sea at 18 UTC of 29 October 2018. Scales are respectively ms^{-1} , m, m.

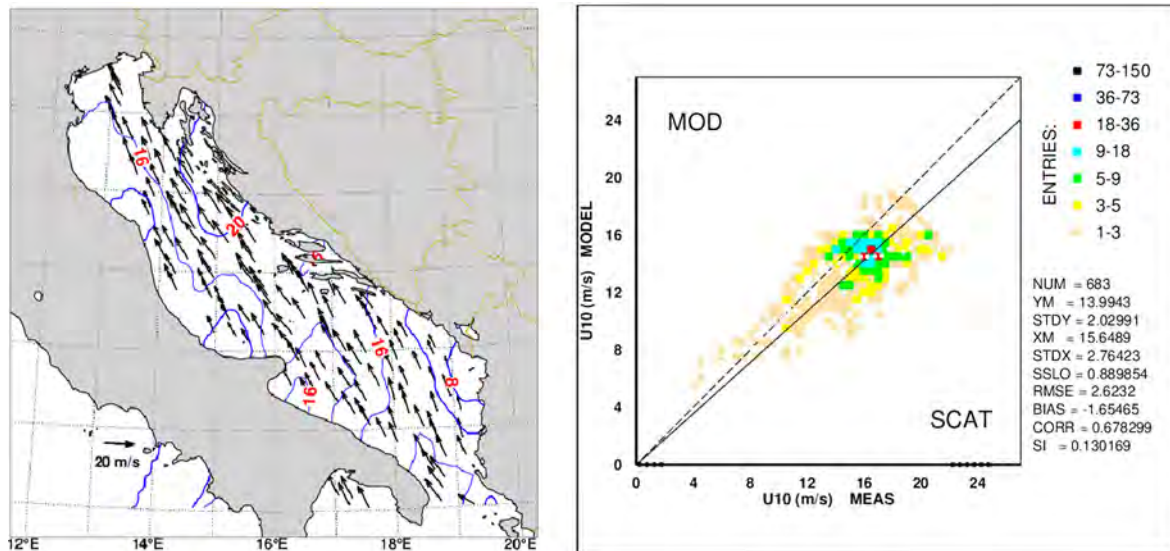


Fig. 5. Left panel: ASCAT-B scatterometer data in the Adriatic Sea at 19.10 UTC 29 October 2018. Only part of the data is shown for better visibility. The right panel shows the best-fit between ECMWF 10 m wind speeds and the ASCAT-B data.

several vertical levels to obtain a general view of the overall situation, for our analysis in this paper we present the surface maps that best illustrate the conditions in the Adriatic Sea.

4.3. Waves

For wave modeling we used the WAM model, amply described in the literature; see the classical Komen et al. (1994) and the ECWAM: IFS documentation CY45R1, part VII at <https://www.ecmwf.int/en/forecasts/documentation-and-support/changes-ecmwf-model/ifs-documentation> for a more specific reference to the details of its use at ECMWF. Performance is available at <https://www.ecmwf.int/en/elibrary/18746-evaluation-ecmwf-forecasts-including-2018-upgrade>. Aiming at a higher resolution than the 14 km available from the Centre global model, for the Adriatic Sea, as regularly done for the local operational activity (Bertotti et al., 2011), WAM (30 frequencies, 15° resolution) was run with 1/12° resolution and suitably corrected ECMWF wind speeds (more on this in the next section). Full fields, and in particular the data at the ISMAR oceanographic tower, have been made available at hourly intervals. 2D spectra are saved at a specified number of points, including of course the tower.

Following the Janssen (1991) approach and related further developments in the above cited reference, the ECMWF fully coupled forecast system implies a continuous exchange of information among atmosphere, wave and ocean. This is clearly not the case when running our Adriatic wave model. However, with very good approximation this is not relevant because the ECMWF wind we used, albeit with slightly lower wave heights, has already taken the interaction into account.

4.4. Tide and surge

Sea level forecast for Venice implies modeling both the sea and the lagoon. Granted the astronomical component, the storm surge contribution is evaluated with the SHYFEM model (Umgiesser et al., 2014) over a spatial domain covering the Mediterranean Sea. SHYFEM solves the 3D primitive equations vertically integrated over multiple z-layers and horizontally over an unstructured grid. Sea level boundary conditions at Gibraltar are provided by the IBI forecast system (http://marine.copernicus.eu/services-portfolio/access-to-products/?option=com_csw&view=details&product_id=IBI_ANALYSIS_FORECAST_PHYS_005_001, Sotillo et al., 2015). The model has been run with ECMWF surface wind stress and atmospheric pressure fields. To take the white-

capping input to current into account, the full wind stress to the ocean has been used (see ECMWF, 2018).

Not part of this paper, but relevant for the final discussion on the reliability of the sea level forecast in Venice, using the corresponding marine conditions SHYFEM is extended to cover also the lagoon (Ferrarin et al., 2010, 2013), mostly shallow (one meter average depth), but with a network of deeper canals (Madrcardo et al., 2017).

5. Modeling results.

Fig. 4 provides the wind, wave and surge fields in the Adriatic at 18 UTC of 29. We use this time instead of 19 UTC (peak conditions) because, as soon explained, the meteorological model anticipates at between 18 and 19 UTC the passage of the cold front, which affects all the marine fields.

5.1. Wind

The wind evaluation is based on ECMWF operational forecasts. These wind speeds are generally underestimated in the Adriatic Sea. In general, the fields have too low speeds for the first 100–200 km when the wind passes from land to sea. Cavaleri and Bertotti (2004) and Signell et al. (2005) provide clear evidence of the problem. Incidentally, we point out this is not typical of only the ECMWF wind fields (Andy Brown, personal communication). Because the problem is permanent and repetitive, a correction is possible when used for local operational applications (see the previous section). Being fetch dependent, the underestimation, and the consequent correction, vary with the wind direction, in practice if across or along the Adriatic main axis. For the present Tco1279 resolution, 9 km, a 1.16 average enhancement is normally used for ISMAR operational activity, expected slightly in excess for sirocco, in defect for bora. However, for this specific devoted study we wished a more precise figure. Two facts helped in this respect: (1) the 29 October storm in the Adriatic Sea was dominated by a uniform, steady unidirectional sirocco wind (see Fig. 4a) blowing from S-E to N-W, (2) the pass of the ASCAT-B satellite borne scatterometer all along the basin at 19.10 UTC providing a perfect check of the model data (see Fig. 5, left panel). The resulting fit (right panel) suggests a 1.11 correction factor for the ECMWF wind speeds. This is fully consistent with previous experience. As for direction, the model wind is on average directed 2° clockwise with respect to the scatterometer data. Further, although at a point, verification in this respect has been

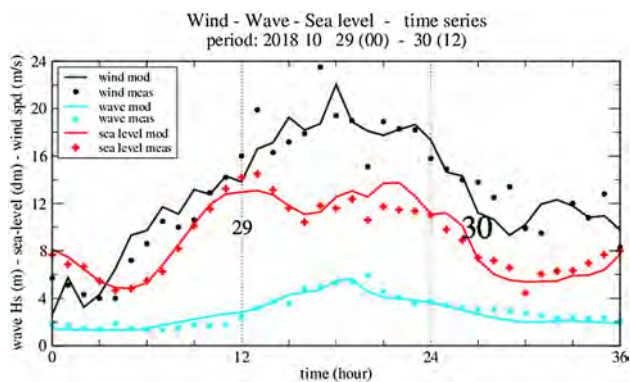


Fig. 6. Comparison between wind speeds, significant wave heights and sea levels measured at the tower (see Fig. 3) and the corresponding model data. Time (hours) goes from 00 UTC of 29 till 12 UTC of 30 October 2018.

achieved with the comparison of the data recorded at the oceanographic tower (see Figs. 1 and 3 for its position). Henceforth, as in the comparison in Fig. 6, our official ECMWF wind speeds will be 1.11 times the original product. We stress that (1) this is a self-standing correction, independent of the wave and surge model results, (2) it is valid for the present event and possibly for all the sirocco storms in the Adriatic Sea. Different corrections may be required in other coastal areas, depending on the local geometry.

Fig. 6 displays the evolution of the storm at the tower, starting in early 29, ending at 12 UTC of the 30. The strong dynamics of the storm, especially in its growing stage, is reflected in the irregular growth of the model wind at the tower and, at a greater extent, the corresponding recorded data (hourly averages on 10-min windows in the figure). We point out that the wind data at the tower have not been corrected for height (CPSM, taken at 18 m – see Section 3) and for the structure influence.

The wind data at the tower are available at a 5-min interval. This allowed to isolate the local passage (see Figs. 1 and 2) of the westerly violent cold front between 19.15 and 19.25 UTC. Direct inspection of the ECMWF hourly maps (forecast issued at 00 and 12 UTC) suggests that the model anticipates the passage of the front of slightly more than 30 min. We will take this into account in judging the wave model results.

5.2. Waves

The wave field at 18 UTC on 29 Oct is shown in panel 4b. It is obviously narrowly concentrated around the mean direction of the wind, the waves pounding heavily on the Venice coastline. We will describe the implications in Section 7. Following both the wind distribution (4a) and the reducing depth moving N, the highest waves are present on the E coast of the basin, still reaching almost 6 m significant wave height H_s at the tower (see Fig. 6). Following the last point in the previous sub-section, note how the model peaks before the measurement.

The measured and model spectral evolutions at the tower are shown in Fig. 7. Referring first to measurements (left panel), we have plotted with a continuous line the growing sea conditions, marked thick at the peak, and indicated with a dash line the decreasing energy spectra. As just pointed out the peak hourly conditions are at 19 UTC. Albeit with a slightly different spectral shape, the model (right panel) provides a similar evolution. Note however the different relationship between the peak and the previous and following spectra as a consequence of the meteorological model leading (by slightly more than 30 min) the passage of the cold front.

As mentioned in Section 3, we lost the signal from the stereo-video system available on the tower at 14 UTC. So we missed the initial intense part of the storm. The highest conditions occurred in any case

when the system could not operate (nighttime). However, we have a very interesting 2D spectrum at 13 UTC, shown in Fig. 8, left panel is the measurements, right is the model. At this stage H_s was ‘only’ 3.2 m. Granted there are some differences in the shape, it is clear that the two spectra are consistent, as also expected from the model-measurement fit in Fig. 6 at this time. The remarkable not trivial detail is the patch of energy moving in opposite direction in the measurements. We will come back to this in Section 7.

5.3. Surge

We have previously mentioned that the geometry and bathymetry of the basin lead in stormy sirocco conditions to a strong enhancement of the surge in front of the Venice lagoon. This is evident in Fig. 4c showing the situation at 18 UTC. As we will discuss in more detail, there is a crucial interplay between astronomical tide and surge. While from the physical point of view we aim at estimating the non-periodic and meteo-dependent surge, the overall “tide + surge” sea level is the one of concern for coastal flooding, and in particular for Venice. On this basis we compare in Fig. 6 the expected and measured sea level at the tower (there is a slight decrease and delay of the tide entering the lagoon – more on this in Section 7 and in the final discussion). The actual sea level peak was reached at 13 UTC, fourth highest historical level of flooding in Venice since 1872, the starting year of the measurements. Note the second sea level peak about six hours later. This point is better appreciated looking at Fig. 9. This provides the astronomical tide, the overall sea level (the same as in Fig. 6) and the resulting surge (the difference, dash line). Note the extent of the surge around 18 UTC, in itself 1.30 m, that only by a lucky optimal phase difference with the astronomical tide did not lead to the by far worst flood in history. The fourth, blue line provides the modeled surge that, with some differences along the growing and decreasing stages, managed to pinpoint time and level of the peak. Note also how the astronomical tide oscillates around a non-zero level. This is actually 26.3 cm (at the time of writing). The reason is historical and practical. This is the reference, at the time correct, mareographic 0 level of 1897. During this elapsed time Venice kept sinking (at different rates) and sea level rising. That mark is now 26.3 cm below the present mean sea level. However, for practical purposes the tidal information are issued with this reference, because that is what accounts for the possible flooding of the different parts of the town.

Having acknowledged the performance of the model for short-term forecasts, for all practical purposes we need to assess model capability to anticipate this information. The issue of predictability over longer durations is now explored.

6. Predictability

The purpose of this section is to assess the capability of the “ECMWF wind + WAM wave + SHYFEM surge” system to correctly forecast the events, in particular the conditions of the 29 October storm. This is done with two separate approaches. First, we focus on the model output at the ‘Acqua Alta’ tower (see Fig. 3) and verify how well ECMWF was able to forecast the local wind conditions. To summarize the wind predictability of the case, Fig. 10 shows a summary of all high resolution (HRES) and ensemble forecasts from ECMWF for 24-h maximum wind gusts valid on the 29 Oct for the location of the tower. The figure also includes the model climatology for the same location and time of the year. In the last forecast before the event the ensemble median was similar to the 99th percentile of the model climate. For the longest forecasts included in the figure (starting from 15 days before the event), the distribution of the ensemble was slightly shifted to weaker gusts than in the model climate, but from eight days before the event (21 October) the distribution started to shift towards higher values. From 23 October and onwards all ensemble medians as well as all HRES forecasts predicted gusts above the 75th percentile of the model

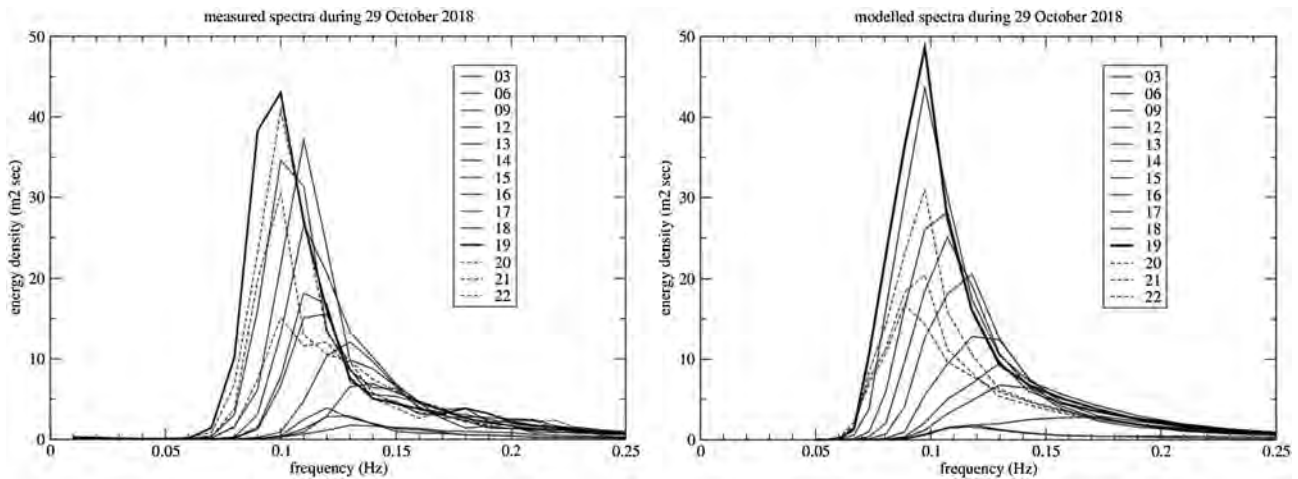


Fig. 7. Hourly wave spectra at the oceanographic tower (from the radar surface profiler – see Section 3). See its position in Fig. 3. Left panel: measured spectra, right one: model spectra. The thin lines show the obvious growing stages of the storm. The thick line is the peak condition. The dotted lines show the progressively decreasing stages.

climate. Note that the maximum recorded wind speed at the tower (1-min average) was 24.8 ms^{-1} with gusts up to 32.1 ms^{-1} . It is clear that a substantial warning in this respect was available six or seven days before the event.

For the second approach we take a more integral view, with a look at the general fields and the related integrated oceanographic results: wave height and surge. Along this line we have issued medium-range (up to several days) oceanographic forecasts starting at different days/times before the event, and checking the results versus the last (a few hours) forecast and the measured data. We have up to ten-day forecasts, using both the 00 and 12 UTC ECMWF model runs. The time interval the ECMWF forecast fields are stored with varies with the lead time: 1 h from 1 to 90 h forecast, 3 h from 93 to 144, afterwards 6 h. We have interpolated in time these fields to have available for each starting time a full forecast sequence of 241 (0–240) hourly fields. While this did not imply any particular problem for waves (the Adriatic Sea wave memory is typically two days), simulating surges requires a longer spin-up. Indeed, for the correct evaluation of all the non-astronomical oscillations in the Mediterranean, hence via the Otranto Strait in the Adriatic, typically at least a month is required (Ferrarin et al., 2013). Therefore the surge model was initialized with a one month simulation using ECMWF analysis data, then shifting at the day of interest to the specific

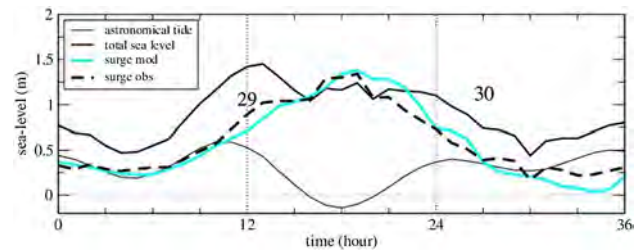


Fig. 9. Astronomical tide, surge and total sea level at the oceanographic tower. See Fig. 3 for its position. Time (hours) goes from 00 UTC of 29 till 12 UTC of 30 October 2018. The blue line shows the model surge. The actual 0 of the astronomical tide is 26.3 cm above the official reference for Venice. See text for explanation. (For interpretation of the references to color in this figure legend, the reader is referred to the web version of this article.)

forecast fields.

An immediate perception of the general meteorological predictability is provided in Fig. 11 showing, for the Adriatic area, the wind forecasts valid for the 29 and issued respectively at 00 UTC of 24, 25, 26, 27, 28, 29. Note that for each forecast we report the conditions at 18 UTC of 29 October. While for this range of forecast the 18 fields are all

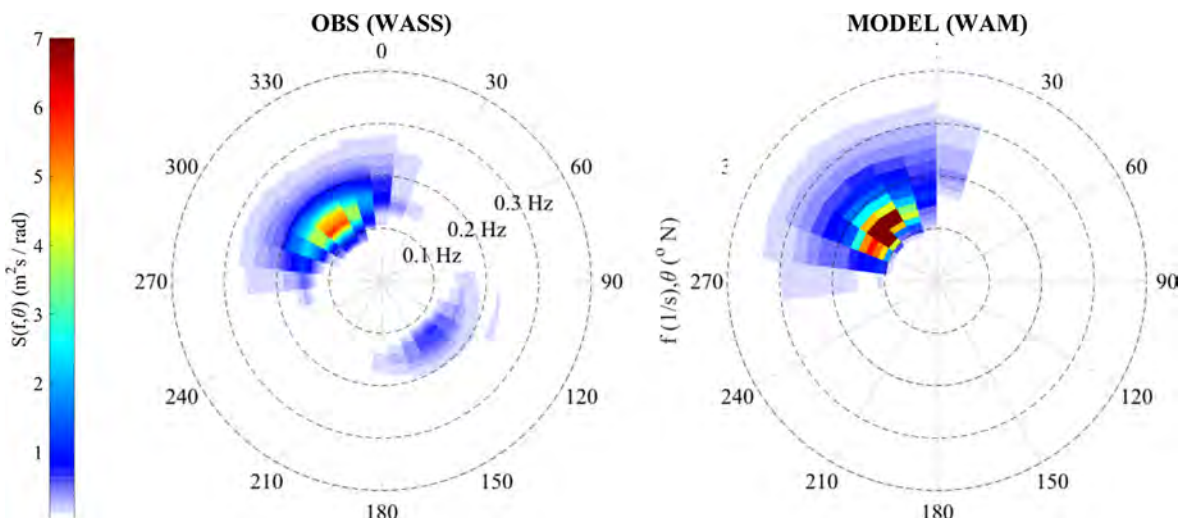


Fig. 8. 2D spectra at the oceanographic tower at 13 UTC of 29 Oct. See Fig. 3 for its position. Left, measured spectrum (with the video stereo system); right, model spectrum. Note the opposite propagating waves in the measured spectrum.

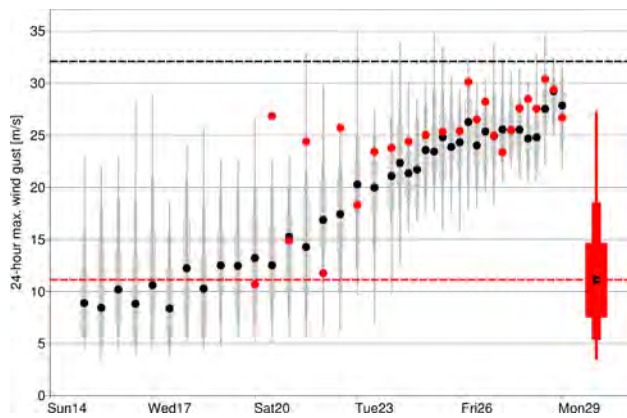


Fig. 10. The box-and-whisker plot shows the evolution of forecasts for 24-h maximum wind gusts on 29 October for the location of the tower for different starting dates. See Figs. 1 and 3 for its position. The grey (red) bars indicate the 1st, 10th, 25th, 75th, 90th and 99th percentile for the ensemble forecast (model climate of the ensemble), and the red dots the HRES forecast. The black dots are the mean of the respective distributions. The 32 ms^{-1} dashed line is the peak gust recorded at the tower. (For interpretation of the references to color in this figure legend, the reader is referred to the web version of this article.)

close to the worst conditions, hence the fields in Fig. 11 are representative of the storm, this is not necessarily the case for earlier forecasts. This is crucial for sea level warnings, as mentioned in the previous 5.3 sub-section and we will further elaborate in the final discussion. The combined information, error in range and time, is provided in Fig. 12. We consider the recorded maximum surge and H_s at the tower, 1.46 and 5.92 m, respectively, and show how the corresponding forecasts progressively approach the measured values. The errors in time are provided by the horizontal bars. We see that up to five (six for the surge) days earlier there were indications of a severe event (H_s close to 4 m, surge to 1 m), with potential warning up to eight days forecast range. As Grazzini (2007) and Cavaleri et al (2010) discuss for the 1966 and 1979 historical cases, an extended predictability seems to be a characteristic of these strong events that, on a more general perspective and as described in Section 2, follow a well-defined meteorological pattern typical of the Western Mediterranean basin in the Fall. More on this in the final discussion.

7. Coastal physics

Till now we have focused our attention on modeling results for the Adriatic Sea, checking them with the tower data, 15 km offshore. It is time to zoom more on the area shown in Fig. 3, exploring the consequences of a strong storm on the coastal environment. We touch in sequence four subjects: coastal set-up, modeling the sea level in the lagoon, the passage of the front, and the implications of the opposing waves found in Fig. 8.

7.1. Coastal set-up

The storm of 22 December 1979 destroyed part of the upper-structures of the tower (they were two meters lower than now), including the onboard energy supply system. Only two records survived thanks to mechanical recording: wind and sea level. The latter, first assumed to be wrong (poor working of the instrument) because of the sea conditions, turned out to be the first solid evidence (coastal-offshore sea level) of wave set-up (Longuet-Higgins and Stewart, 1964; Bowen et al., 1968). See Bertotti and Cavaleri (1985) for a full description of the data and related modeling.

The 1979 and 2018 storms were of comparable intensity, H_s in particular. Hence a similar effect is to be expected for the 2018 storm. This is clearly shown in Fig. 13 where we plot the sea level recorded at

the tower and at the coastal tide gauge located (Fig. 3) 2 km offshore, at the end of the Lido jetty. The relationship between the wave heights at the tower and the more than 25 cm ‘Lido – tower’ sea level difference is evident. However, this is only part of the story. As we will soon discuss in Section 7.3, wind has a role as well. In equilibrium conditions a surface wind stress towards the coast must correspond to a sea level gradient in the same direction. This is inversely proportional to the local depth, hence quickly growing approaching the shallower coastal waters. Therefore part of the cited ‘coast-tower’ sea level difference is due to wind as well. However, wind speed, and the related wind-sea distribution, were substantially decreased at the end of the day. More importantly, the wind direction changed after the passage of the front, then blowing from the South, hence obliquely to the coast. At the same time swell kept pounding the coast, hence the parallel decrease also on the 30 of the wave height and the coastal set-up.

Two more things need to be pointed out. First, the sea level at the Lido jetty is the one of relevance for Venice, forcing the input to the lagoon. Second, given the depth at the jetty end, a much higher set-up was present at the coast, as documented by the reported extended damages.

7.2. Modeling the sea level in the lagoon

As described in Section 4.3, the SHYFEM model is extended to the lagoon to model the related sea level distribution. The mostly shallow (1 m) water of the lagoon makes the surge distribution very sensitive to wind. This is clearly shown in Fig. 14 where the modeled water level distribution in the coastal and lagoon is plotted. Knowing the wind direction, from S-E to N-W, the dominant effect of the wind, better said, of the local wind stress, on the overall water level distribution is immediately recognized. Both in the sea and the lagoon the isolines are practically perpendicular to the wind direction. An exception is the northern area of the lagoon where the hysteresis of the system, with the implied delays, dampens the higher oscillations present in the other parts of the lagoon.

7.3. Front passage

In Section 2, describing the evolution of the meteorological situation on northern Italy, we have mentioned how after 18 UTC an energetic cold front crossed the Apennines and advanced over the Northern Adriatic Sea. Indeed, after several hours of continuous sirocco, the wind record at the tower, at 5-min interval, documents the passage of the cold front at 19.15 UTC (wind changes direction by 40° clockwise). The tide gauge data strongly suggest that the change implied a rapid readjustment of the sea level distribution in the coastal area, including the tower.

Fig. 15 shows the sea level, at 5-min intervals, recorded at the tower, the Lido gauge and at the Chioggia inlet. See Figs. 3 and 14 for the local geometry. The dominant feature is the drop in sea level, more than 20 cm in 10-min, at the tower, that happened soon after the front passage (19.15 UTC, 135 min in Fig. 15). Our interpretation is as follows. With wind blowing and waves moving normal to the coast, there is a pile up of water at the coast (just discussed in Section 7.1). At any instant the “towards the coast up-slope” is supported partly by the wave set-up, and partly by the local wind stress. A sudden change of wind direction changes abruptly the supporting surface stress. The system (the sea level distribution) must adapt to the new situation, and the new equilibrium implies a lower slope with a consequent rapid redistribution of the related water mass. Granted the lack of details in the forcing, we suggest this is a unique case where we have, in an indirect way, physical evidence of, hence the possibility to estimate, the surface stress to the ocean.

Our interpretation of the front passage is supported also by the records at Lido and Chioggia inlets (Fig. 15). Malamocco data are not available because of flooding of the gauge well in heavy sea conditions.

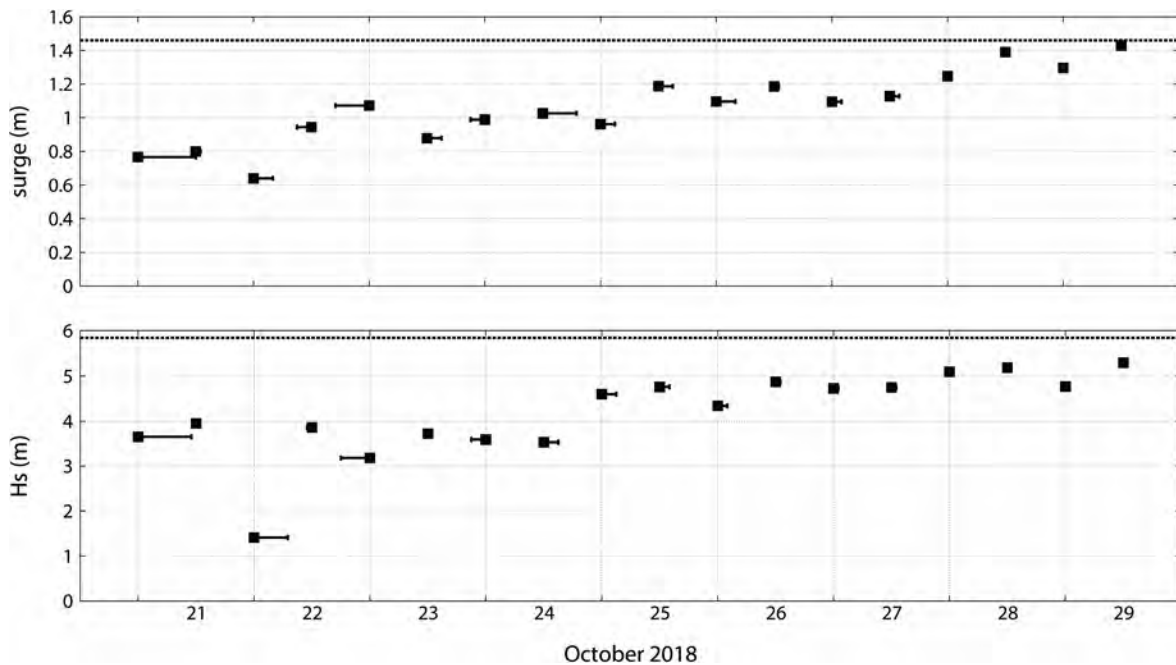


Fig. 12. Predictability of the 29 October 2018 event. The two panels show the corresponding surge and significant wave height forecasts issued at different dates and time. The horizontal bars show the errors in timing the worst 29 October 19 UTC conditions. The two horizontal dashed lines show the respective measured values.

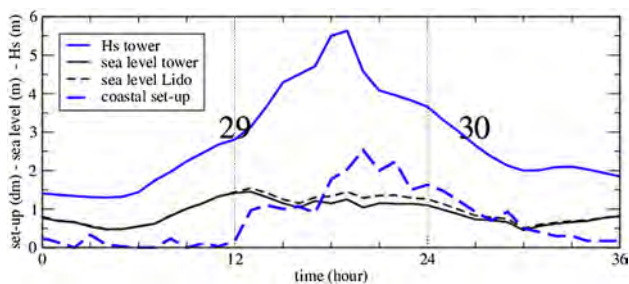


Fig. 13. Sea level at the coast (Lido inlet) and the tower. See Fig. 3 for their position. The other two lines show the respective difference (coastal set-up) and the significant wave height at the tower. Time (hours) goes from 00 UTC of 29 till 12 UTC of 30 October 2018.

attracted our attention. Excluding any local dynamical non-linear behavior, the simplest explanation was a reflection from the coast. We were a bit skeptical because the 1/1000 bottom slope toward the coast with a very flat final beach does not suggest an effective reflection. However, at the same time we were provided with some seismometer data from Padua University, 40 km inland. The particularly strong signal of 29 and 30 October is shown in the left panel of Fig. 16. It is difficult not to think of an association with the contemporary storm. Inland seismometer records of offshore wave conditions, if strong enough, are a known fact. Starting with the 1951 basic dissertation by Longuet-Higgins on the subject, this was taken up again in recent times by Kedar et al. (2008) and Arduin and Roland (2012), among others. However, for waves approaching the coast to generate inland microseisms a certain level of reflection by the coast is required. We thought this unlikely on the Venice beach. However, the correct link was provided by the spectrum in Fig. 8, showing beyond any doubt the presence of reflected waves. We can only hypothesize that the heavy wave conditions, supported also by the coastal set-up, moved the wave breaking and run-up more up the beach, with a potential reflection enhanced by the out of season sandy dunes erected to protect the tourist infrastructure. The typical link between sea waves and seismometer signal implies that the seismic wave has a double frequency with respect to waves. The right panel of Fig. 16 shows the seismometer

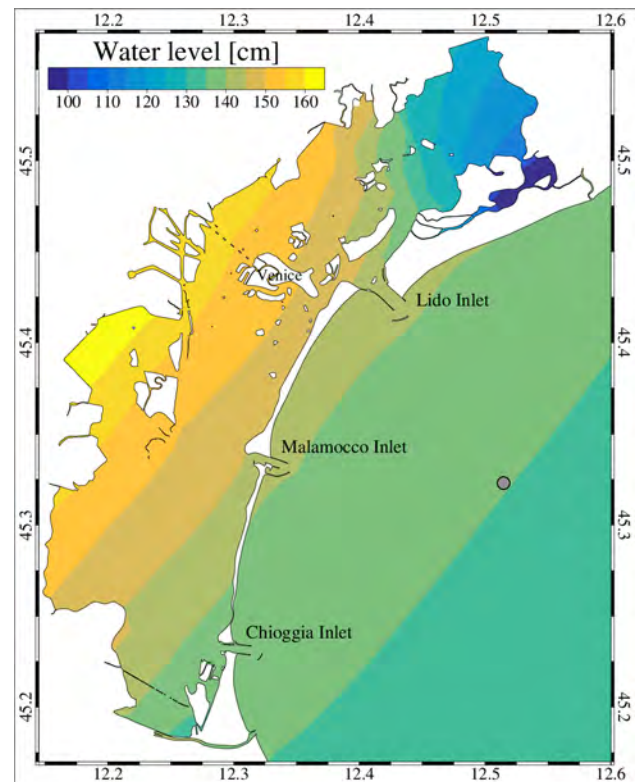


Fig. 14. Modeled sea level distribution at 18 UTC 29 October 2018 in the area off the Venice coastline and in the lagoon. See Figs. 1 and 3 for their position. The small circle shows the tower position.

spectrum at the peak of the storm. The peak at 0.2 Hz (5 s period, half of the period of incoming waves) is unmistakable. However, we warn that 5 s is also close to the natural period of the seismometer, but the much stronger signal following the energy of the storm is quite clear. Not shown, in the seismometer spectra before and after the storm the seismometer spectral peak is drastically lower and at a lower frequency.

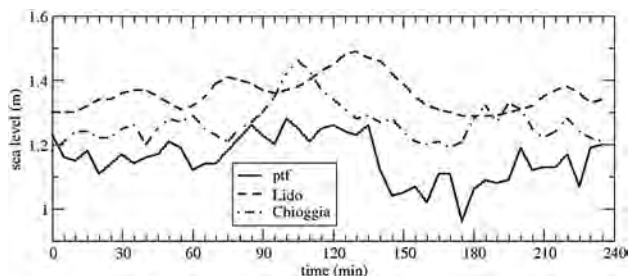


Fig. 15. Time history (17–21 UTC 29 October 2018) of the recorded sea level at the tower (ptf) and Lido and Chioggia inlets. See Fig. 3 for their positions.

8. The highest wave heights

In practical applications, as e.g., the cited ECMWF forecast activity, the standard output of the wave model includes the 2D spectral distribution in space and time. Given the wave conditions at known time and location, an important coastal design piece of information is the height, or crest height, of the expected largest wave. See Benetazzo et al. (2017), Cavaleri et al. (2017) and Barbariol et al. (2019) for a discussion on the matter. The availability at the tower of both detailed wave measured data (stereo video system and single point radar – see Section 3) and model spectra allows a keen verification of the theoretical approach in extreme sea state conditions.

The left panel of Fig. 17, based on the wave conditions at 13 UTC, compares the expected (blue line) maximum crest height and profile derived using the WAM model spectrum with (dashed line) the corresponding result derived from the stereo system. The shadow represents the confidence limits associated with the measurements. The considered space and time intervals are 35 m² and 120 s respectively. At this time the significant wave height was 3.2 m. The agreement of the observed and modeled profile allows inferring the profile of the wave with the largest expected crest height at 19 UTC, close to the heaviest conditions at the tower. This is shown in the right panel for 35 m² and 3600 s, the longer time interval allowing an estimate consistent with the duration of the peak conditions. The height reached by the crest of the largest expected wave (7.90 m) is compared to the height of the

damaged structure suspended below the tower deck n. 2. This deck corresponds to the level of the outgoing horizontal platform (Fig. 3) at the second floor of the tower. The nominal height on the mean sea level of the suspended structure is 8.40 m, reached by the wave crests during the storm because of the higher sea level present at that time. This is why in the figure the waves are relative to a sea level of + 0.94 m, instead of mean sea level.

Fig. 18 provides a similar information based on the observed single point radar data available at the peak of the storm. During the 18–19 UTC radar record (7200 data at 2 Hz) several apparently anomalous crest heights were recorded that prompted a keen verification of the record. The one in the right panel is an example. Excluding (by direct inspection) spikes and other anomalous reasons as possible explanations, we explored the related crest height distribution. The result is in the left panel. Here we have plotted three distributions, in increasing level of non-linearity of the process, respectively Rayleigh, Tayfun, and Tayfun and Fedele (2007), this last one (TF) accounting for skewness and kurtosis of the sea state (0.41 and 3.37, respectively). Looking at the figure, it is obvious that the data follow the TF distribution, but only up to a certain point, after which we find a few “anomalous” very high values. We do not have an explanation for them. We stress that the commonly used definition of “anomalous” implies in itself something exceptional, something that by instinct we tend to associate to a single (the so called freak) event. However, this is no more the case when we have three or four of them out of 360 waves. If, as this case, this is not due to an instrumental error, physics must be at play, a physics we do not fully understand. We will comment further on this in the last section.

9. Long term statistics

When a rare, especially if damaging, event takes place, it is natural to ask how rare was it, or what is its expected return interval. Several attempts have been performed to fit the Venice surge data with extreme distributions, and a large range of different results has been obtained (Marani, personal communication). Obviously the 29 October event will lead to new estimates. Rather than entering this game, we want to look at the problem from a different perspective. Clearly the origin of

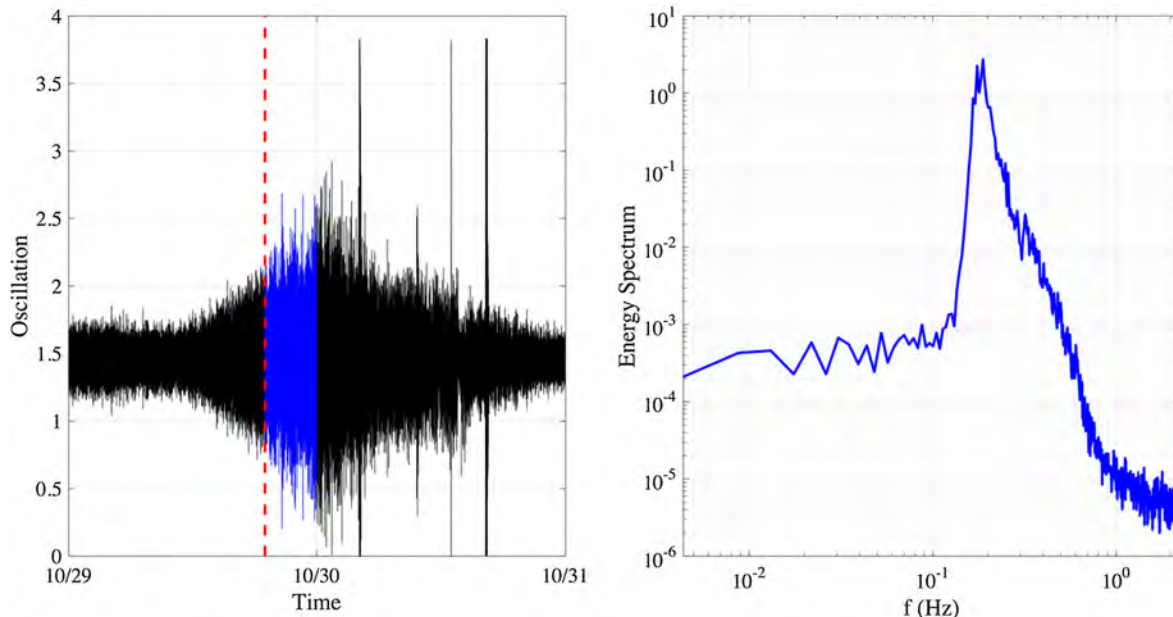


Fig. 16. Left panel: record (29–30 October 2018) of the seismometer at Padua University, 40 km inland with respect to the coast. The red dashed line shows the time 19 UTC when H_s peaked at the Acqua Alta tower, and the blue line the excerpt from 19 to 24 UTC on 29 October. Right panel: energy spectrum of the seismometer oscillations recorded from 19 to 24 UTC on 29 October. (For interpretation of the references to color in this figure legend, the reader is referred to the web version of this article.)

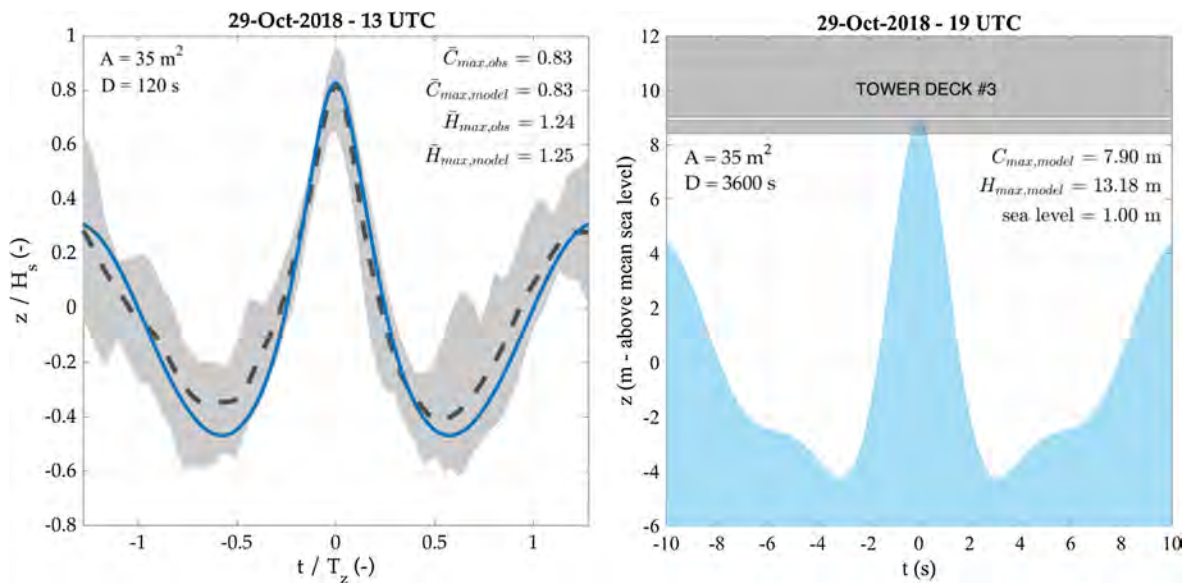


Fig. 17. Largest wave heights. Left panel: normalized profile of the expected largest wave at the tower at 13 UTC, from stereo observations (black dashed line) and model estimate (blue solid line). Space and time intervals considered are 35 m² and 120 s. The gray region represents the confidence limit of the observations. Right panel: profile of the wave with the largest expected crest height at 19 UTC, from model estimate, compared to the highest tower deck that was damaged. Space and time intervals considered are 35 m² and 3600 s. Sea level at the time was 1.00 m. (For interpretation of the references to color in this figure legend, the reader is referred to the web version of this article.)

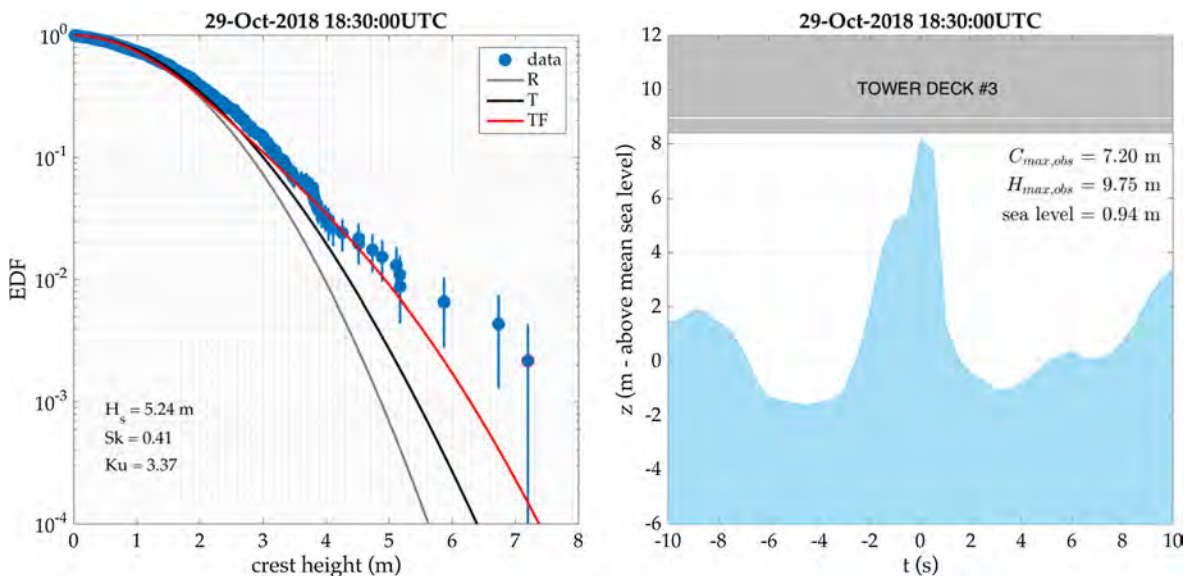


Fig. 18. Largest wave heights. Left panel: exceedance distribution function (EDF) of the observed crest heights (data, blue dots), from the single point radar (3600 s). Theoretical EDFs are plotted for reference (R: Rayleigh, T: Tayfun, TF: Tayfun-Fedele). Right panel: profile of the wave with the largest crest height, compared to the highest tower deck where damage was reported. Sea level at the time was 0.94 m. (For interpretation of the references to color in this figure legend, the reader is referred to the web version of this article.)

everything is meteorological, but usually researchers pay a special attention to measured data. For our interests the two main parameters are surge level and significant wave height H_s , in particular in front of Venice. Thinking about the input to the corresponding models, wind and surface pressure, wave height appears as a more general parameter because it is representative of the conditions on the whole Adriatic basin, while, as we have seen, surge is highly dependent on the conditions in the last tens of kilometers near the coast. In any case, surge or H_s , the peculiar point we want to call the attention to is how the 1966, 1979 and 2018 cases fit in the general distributions. Using, for the specified reasons, H_s as an example, we consider the distribution of its peak values for all the 1979 to present storms, based on the historical directional wave dataset recorded at the Acqua Alta tower, as

documented in Pomaro et al. (2018). We then find a regular, continuous distribution up to 4.6 m, after which a void before until the two isolated values 5.92 (2018) and 6.0 (at least from the 1979 hindcast and the damages to the tower). In any case a similar, more quantified argument can be made for the measured surge, with 1.25 and 1.50 m (respectively for 1979 and 2018). The distributions are shown in Fig. 19, where we plot the number of occurrences for each wave height and surge range. Although less so for surge, it is clear that the two cited storms stand by themselves, certainly so for wave heights that, as we mentioned above, are more significant for the general meteorological situation. The distribution is even more singular if we take into account the 1966 storm, where surge (1.66 m) and wave height (much larger than 6 m) were the highest ever remembered. There were enormous damages on coastal

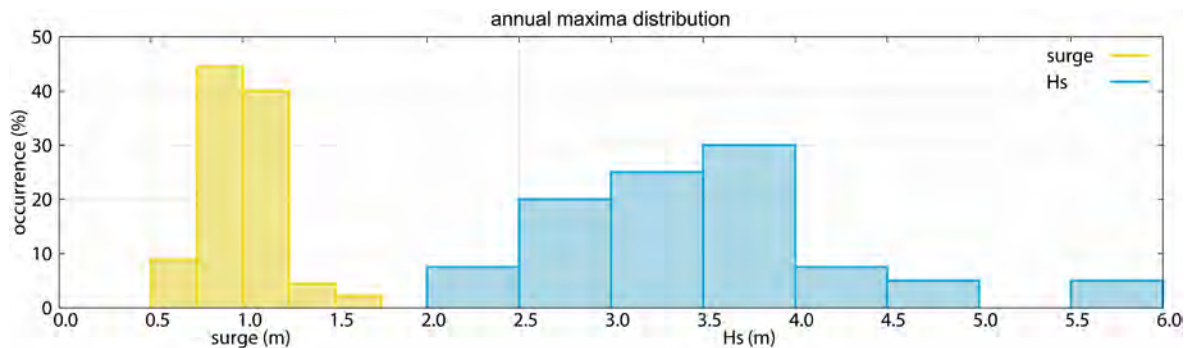


Fig. 19. Statistical distributions of the maxima surge η and significant wave height H_s values for all the events for $\eta > 0.5$ m and $H_s > 2.0$ m. The period considered is 1979 to present.

structures. As an example, the last 200 m of the six jetties at the lagoon inlets were not existent after the storm.

We do not have, and as far as we know no one has, an explanation for this anomalous distribution. Stimulated by this result and on a completely different perspective, we wonder if these storms belong to the same kind, or family, of storms of the other milder events. Should this not be the case, different statistics would apply to the two families of events. It is clear that the problem is meteorological, because this is the genesis of both surge and waves. A reason for arguing this point is also that, apart from the 2018 explosive cyclogenesis, the three storms have almost identical genesis and meteorological pattern. This is of course a point to keep in mind. We do not have the answer, but at the same time we do not think that invoking only random chance is the answer as well.

10. Discussion

Following the large-scale storm that affected Northern Italy at the end of October 2018 (large waves also in the Ligurian Sea (see Fig. 1) and the strong wind on the Eastern Alps), in this paper we focus on the sub-scale events on the Adriatic Sea. The reason is that these sub-events deserve by themselves a devoted attention, on one hand for the level of the storm and its implications, on the other hand because the contemporary availability of both offshore and coastal data has allowed specific considerations on several aspects of coastal processes. We discuss in sequence the relevant aspects of our results.

The storm

In one way the storm was typical of the Fall. In this period, following the often still summer-like position of the Azores anticyclone and the growing cold inputs from Northern Europe, a cold tongue of relatively low pressure air protrudes from France into the Western Mediterranean basin. If cold air bursts in from the Gulf of Lion (see Fig. 1) on this area, the strong contrast with the still warm water leads frequently to the formation of a cyclogenesis. In turn, especially if constrained by a high pressure on the Balkans, this leads to strong S-E (sirocco) winds in the Adriatic Sea, and hence to high waves and surge in front of the Venice coast. In the present, 29 October 2018, case the overall pattern was complicated, and in itself unique, because of the intensity of the explosive cyclogenesis, the consequent (cited above) storms on the Ligurian Sea, the intense storm in the Adriatic Sea, and the strong winds on Eastern Alps.

Predictability

Previous studies of these kind of storms, especially if very intense (see, among others, Cavaleri et al., 2010), suggest a possible good level of predictability. Indeed the general meteorological pattern is typical of major precipitation events in the Mediterranean in the fall, and

therefore we should expect to be able to anticipate its development (Grazzini, 2007). Strong wind gusts, at the extreme of the climatological distribution, were available in the forecasts up to eight and nine days ahead. Our oceanographic experiments with forecasts up to ten days before the event show this is indeed the case. Good quality predictions were available up to five or six days before the event. Its strength may have been underestimated, less so at shorter lead times, but the warning of a significant event was there. Mild warnings were available till eight days ahead. This, up to six days ahead as tested at the time, is consistent with the results previously obtained (Cavaleri et al. (2010)) for the other two similar events of 1966 and 1979. However, this is not the case for the explosive cyclogenesis we have seen in Fig. 2b and described in Section 2, whose small scale and strong radial gradients made it very sensitive to also small scale, hence less predictable, details of the fields.

Modeling

The wind fields on the Adriatic Sea are strictly associated to the overall meteorological structure. In the present case we were fortunate to have the pass of a scatterometer at the peak of the storm, with a consequent direct verification of the model surface wind field. This confirmed what is already known and regularly considered in our Adriatic operational activity: the ECMWF wind fields are locally geometrically correct, but slightly underestimated in wind speed. This is a known deficiency with offshore blowing winds, hence relevant in enclosed seas and coastal environments, notably present also in the UKMO and NCEP surface products (personal communication). This underprediction is regularly taken into account in our local operational activity, but the passage of ASCAT-B allowed a more specific correction. We stress again this is uniquely a wind correction, based on objective data, independent of the following wave and surge results. With the correct wind, waves and surge were very close to the respective measured data, slightly less so for the significant wave height, the difference possibly related also to the confidence limits of the measurements.

Timing of the cold front

The development of the general meteorological pattern is well forecast by the meteorological model. This is less the case for the strong cold front. Indeed it is not easy to pinpoint the correct dynamics of these very strong mesoscale events. This is true in particular for their translation speed. The high frequency (5-min) data at the tower clearly show that the model anticipates the passage of the front by more than 30 min, with a consequent positional error of 20 or more kilometers. This is clearly seen comparing the 19 and 20 UTC maps (not shown) versus the tower and coastal wind and tidal data. This time shift needs to be taken into account when comparing general model and measured data.

Surge

The map in Fig. 4c and the coastal set-up in Fig. 13 show very clearly how the surge is concentrated (under sirocco conditions) in the last tens of kilometers before the Venice coast. The consequent strong spatial gradients hint to the difficulty of identifying the correct surge for the estimate of the possible Venice flood. The relevant value is not the one at the coast, but the one two kilometers offshore, at the sea exit of the jetties bordering the inlets to the lagoon. Two things need to be pointed out. First, the set-up at the coast is consequently much larger than the one at Lido shown in Fig. 13. Second, the lagoon has then its own dynamics that, only hinted to, but not dealt with, in this paper, needs to be properly modeled.

Flooding in Venice

The actual sea level, in Venice as everywhere else, is the addition of the just mentioned surge and the regular astronomical tide. We stress the crucial point of the relative timing between the two components. As mentioned in Section 5.3, on October 29 we were very fortunate because the two components were six hours out of phase (out of a 12 h cycle), and indeed the flood peak happened with only less than half a meter surge contribution. Had the 1.54 m surge happened a few hours before, conditions would have been disastrous.

This takes us to the subject of sea level predictability. As stressed in the first two items of this section, we can rely on a sufficient level of predictability for what concerns the strength of the storm, but timing is another matter (see in this respect Fig. 12). For three- or four-day forecast horizon, an error of a few hours (out of 72 or 96) is considered negligible for most practical aspects. However, such an error may have dramatic impacts on the expected overall sea level because of surge timing with respect to the astronomical tide. The only solution is to work with ensemble forecasts, providing the statistical distribution of the combined possibilities.

Offshore and coastal data

The availability of measured data at the offshore tower and at the coast has made evident the relevance of the physics of coastal hydrodynamic processes for local modeling. The substantial sea level differences between the 15–2 = 13 km distant locations are associated to (1) the wave set-up due to the progressive bottom induced breaking moving to progressively shallower waters while approaching the coast, (2) to the surface up-slope towards the coast associated to the surface wind stress acting on relatively shallow depths. In particular the passage of the cold front has made evident, via the quick collapse of the sea level at the coast and in particular at the tower, the role of wind stress in keeping the water pushed towards the coast. Having, although without all the necessary details, the wind fields before and at the passage of the front, in principle we should be able to derive the actual wind stress, a notorious subject of strong debate. The question we tackled, although in an approximate way, is if the surge model is capable handling such a situation. The test performed, halting the wind at the time of the documented front passage, showed a decrease of the sea level at the tower position, but by only a fraction of what shown in Fig. 15. We suspect that, fitted to the historical data, hence without the cited particular scenario, the model cannot handle this strong gradient situation. We suspect this to be a characteristic of most coastal surge models, and we put our data at disposal for anyone keen to test his/her model in this rather unusual situation.

Maximum wave and crest heights

It is obviously of interest to be able, given the spectral conditions, to derive the expected maximum wave and crest heights. We were able to verify our approach using the 13 UTC data, when both video stereo

record and model spectrum are available. Indeed the theoretically derived (from the spectrum) maximum wave profile fits very well the measured data. We have then estimated the corresponding profile for the peak conditions at 19. The resulting crest height (+7.90 m) is consistent with the damage reported at the tower. We are here close to the depth induced limit breaking ($0.73 \times \text{depth}$, Battjes and Janssen, 1978), as suggested also by the shape of the previous and following troughs. However, we believe such a limit cannot be taken as a universal law. The point is that there is a transient when approaching a breaking condition. Therefore, while true on average, we do not consider the Battjes and Janssen limit as a physical limit to the locally possible wave and crest heights.

11. Summary

We itemize our main findings as follows:

- (1) The storm of 29 October 2018 provided, despite its initial commonly observed structure, a rather unusual development that led to extreme conditions on Northern Italy, in particular the Adriatic Sea.
- (2) The availability of detailed coastal and offshore observations in the Northern Adriatic Sea provides a unique data-set allowing a keen study of the local physical processes.
- (3) The ECMWF winds are of high quality, but, as supported by previous studies, slightly underestimated in the enclosed seas, in particular the Adriatic Sea. Regularly addressed in the local operational activity on the base of long term comparisons, for this storm a posteriori the problem has been eased by the availability of scatterometer data. We point out that the problem is not typical of only the ECMWF data.
- (4) Using the corrected winds from ECMWF forecasts, the wave and surge models provide results consistent with the measurements.
- (5) A non-negligible sea level difference is found between the tower and the coastal gauges (lower at the tower). We associate this to the coastal set-up due to wave breaking and surface wind stress.
- (6) The data suggest that the passage of the cold front, with a consequent change of the surface wind stress, leads to a sudden (order of minutes) collapse of the local sea level anomaly, both at the coast and at the tower. Implicitly this offers the possibility of an indirect estimate of the surface wind stress. However, a detailed analysis of the ensuing temporal and spatial variability will require a much more detailed (kilometers and minutes) description of the local transient fields. We plan to put the related data at disposal for tests by other models.
- (7) We found a good predictability of the storm, with substantial warnings up to 5 or 6 days ahead, less accurate at 7 or 8 days ahead. The specific wind at the tower position, including gustiness, was already high in the forecast of six or seven days ahead. However, this concerns more the general pattern, hence the sirocco on the Adriatic Sea. It is less the case for the development of the explosive cyclogenesis on the Western Mediterranean Sea.
- (8) We have evidence of reflected waves from the coast. The resulting partially standing waves are associated to an enhanced seismometer signal recorded during the storm at Padua University, 40 km inland.
- (9) The three highest storms in the last fifty years or so do not appear as possible extremes consistent with long term historical distribution. Each one of them appears as the once in a while event. This is unlikely. We suggest the possibility that they belong to a different family of events.

Declaration of Competing Interest

None.

Acknowledgements

L.C. and L.B. highly appreciate the hospitality of ECMWF whose data have been essential for the present study. All the meteorological data used in this study are the product of ECMWF. The maps of Figs. 2 and 11 have been plotted by Enrico Sambo of the CPSM (Tidal Forecast Centre) in Venice. The seismometer data have been provided by Andrea Battistella of Padua University whom we thank for calling our attention on the matter. A.B. acknowledges the support from the Copernicus Marine Environment Monitoring Service (CMEMS) LATEMAR project. The basic image for Fig. 1 has been provided by the SeaWiFS Project, NASA/Goddard Space Flight Center, and ORBIMAGE. The one for Fig. 3 has been taken from the NASA Earth Observatory images by Jesse Allen and Robert Simmon, using Landsat data from the U.S. Geological Survey. All the data and results used and reported in this paper are available from the authors. Following the rules of the European Centre for Medium-Range Weather Forecasts, all the data derived from their archive must be asked to the Centre. Robert Jensen and two other anonymous reviewers have provided useful suggestions. We wish to thank in particular two of them (including R. Jensen) who, besides indicating some both general and specific necessary changes, have provided a painstakingly detailed correction, word by word, of our not so perfect English. In this respect we had also the valuable help of Silvio Davison.

Contribution

All the authors have contributed to both the scientific study and the preparation of the manuscript

Appendix A. Supplementary material

Supplementary data to this article can be found online at <https://doi.org/10.1016/j.pocan.2019.102178>.

References

- Ardhuin, F., Roland, A., 2012. Coastal wave reflection, directional spread, and seismoacoustic noise sources. *J. Geophys. Res.* 117 (C00120), 16. <https://doi.org/10.1029/2011JC007832>.
- Bajo, M., Medugorac, I., Umgiesser, G., Orlić, M., 2019. Storm surge and seiche modelling in the Adriatic Sea and the impact of data assimilation. *Quart. J. Roy. Meteorol. Soc.* 1–15. <https://doi.org/10.1002/qj.3544>.
- Barbariol, F., Bidlot, J.-R., Cavaleri, L., Sclavo, M., Thomson, J., Benetazzo, A., 2019. Maximum wave heights from global model reanalysis. *Prog. Oceanogr.* 175, 139–160. <https://doi.org/10.1016/j.pocan.2019.03.009>.
- Battjes, J.A., Janssen, J.P.F.M., 1978. Energy loss and set-up due to breaking random waves. *Proceedings of 16th Conference on Coastal Engineering, Hamburg, Germany*.
- Benetazzo, A., Bergamasco, F., Yoo, J., Cavaleri, L., Kim, S.S., Bertotti, L., Barbariol, F., Shim, J.S., 2018. Characterizing the signature of a spatio-temporal wind wave field. *Ocean Model.* 109, 104–123.
- Benetazzo, A., Barbariol, F., Bergamasco, F., Carniel, S., 2017. Space-time extreme wind waves: analysis and prediction of shape and height. *Ocean Model.* 113, 201–216. <https://doi.org/10.1016/j.ocemod.2017.03.010>.
- Bertotti, L., Cavaleri, L., 1985. Coastal set-up and wave breaking. *Oceanol. Acta* 8 (2), 237–242.
- Bertotti, L., Canestrelli, P., Cavaleri, L., Pastore, F., Zampato, L., 2011. The Heneus wave forecast system in the Adriatic Sea. *Nat. Haz. Earth Syst. Sc.* 11 (11), 2965–2979. <https://doi.org/10.5194/nhess-11-2965-2011>.
- Bowen, A.J., Inman, D.L., Simmons, V.P., 1968. Wave 'set-down' and set-up. *J. Geophys. Res.* 73 (8), 2569–2577.
- Cavaleri, L., 2000. The oceanographic tower Acqua Alta - activity and prediction of sea states at Venice. *Coast. Eng.* 39, 29–70.
- Cavaleri, L., Bertotti, L., 2004. Accuracy of the modelled wind and wave fields in enclosed seas. *Tellus* 56A, 167–175.
- Cavaleri, L., Benetazzo, A., Barbariol, F., Bidlot, J.-R., Janssen, P.A.E.M., 2017. The Draupner event: the large wave and the emerging view. *Bull. Am. Meteorol. Soc.* 98, 729–735. <https://doi.org/10.1175/BAMS-D-15-00300.1>.
- Cavaleri, L., Bertotti, L., Buizza, R., Buzzi, A., Masato, V., Umgiesser, G., Zampieri, M., 2010. Predictability of extreme meteo-oceanographic events in the Adriatic Sea. *Quart. J. Roy. Meteorol. Soc.* 136, 400–413.
- ECMWF, 2018. Part VII: ECMWF Wave Model, IFS Documentation CY45R1, 7.
- Ferrarin, C., Cucco, A., Umgiesser, G., Bellafiore, D., Amos, C.L., 2010. Modelling fluxes of water and sediment between the Venice Lagoon and the sea. *Cont. Shelf Res.* 30 (8), 904–914. <https://doi.org/10.1016/j.csr.2009.08.014>.
- Ferrarin, C., Roland, A., Bajo, M., Umgiesser, G., Cucco, A., Davolio, S., Buzzi, A., Malguzzi, P., Drofa, O., 2013. Tide-surge-wave modelling and forecasting in the Mediterranean Sea with focus on the Italian coast. *Ocean Model.* 61, 38–48.
- Grazzini, F., 2007. Predictability of a large-scale flow conducive to extreme precipitation over the western Alps. *Meteorol. Atmos. Phys.* 95, 123–138.
- Janssen, P.A.E.M., 1991. Quasi-linear theory of wind-wave generation applied to wave forecasting. *J. Phys. Oceanogr.* 21 (11), 1631–1642.
- Kedar, S., Longuet-Higgins, M., Webb, F., Graham, N., Clayton, R., Jones, C., 2008. The origin of deep ocean microseisms in the North Atlantic Ocean. *Proc. Royal Soc. A* 464, 777–793. <https://doi.org/10.1098/rspa.2007.0277>.
- Komen, G.J., Cavaleri, L., Donelan, M., Hasselmann, K., Hasselmann, S., Janssen, P.A.E.M., 1994. *Dynamics and Modelling of Ocean Waves*. Cambridge University Press, pp. 532 pp..
- Longuet-Higgins, 1951. A theory on the origin of microseisms. *Phil. Trans. Roy. Soc. Lond. Ser. A* 243, 1–36.
- Longuet-Higgins, M.S., Stewart, R.W., 1964. Radiation stresses in water waves; a physical discussion with applications. *Deep Sea Res.* 11, 529–562.
- Madricardo, F., Fogliani, F., Kruss, A., Ferrarin, C., Pizzeghello, N.M., Murri, C., et al., 2017. High-resolution multibeam and hydrodynamic datasets of tidal channels and inlets of the Lagoon of Venice. *Sci. Data* 4, 170121. <https://doi.org/10.1038/sdata.2017.121>.
- Peureux, C., Benetazzo, A., Ardhuin, F., 2018. Note on the directional properties of meter-scale gravity waves. *Ocean Sci.* 14, 41–52.
- Pomaro, A., Cavaleri, L., Lionello, P., 2018. 39 years of directional wave recorded data and relative problems, climatological implications and use. *Sci. Data* 5, 180139. <https://doi.org/10.1038/sdata.2018.139>. with supplement dataset: Pomaro, A., L. Cavaleri, A. Papa, P. Lionello, 2018. 39 years of directional wave recorded data at the Acqua Alta oceanographic tower. PANGAEA.
- Rabier, F., Jarvinen, H., Klinker, E., Mahfouf, J.-F., Simmons, A.J., 2007. The ECMWF operational implementation of four-dimensional variational assimilation. I: experimental results with simplified physics. *Quart. J. Roy. Meteorol. Soc.* 126 (564), 1143–1170.
- Signell, R.P., Carniel, S., Cavaleri, L., Chiggiato, J., Doyle, J.D., Pullen, J., Sclavo, M., 2005. Assessment of wind quality for oceanographic modelling in semi-enclosed basins. *J. Mar. Syst.* 53 (1–4), 217–233.
- Sotillo, M.G., Cailleau, S., Lorente, P., Levier, B., Aznar, R., Reffray, G., et al., 2015. The MyOcean IBI ocean forecast and reanalysis systems: operational products and roadmap to the future Copernicus service. *J. Operat. Oceanogr.* 8, 63–79. <https://doi.org/10.1080/1755876X.2015.1014663>.
- Tayfun, M.A., Fedele, F., 2007. Wave-height distributions and nonlinear effects. *Ocean Eng.* 34, 1631–1649.
- Trincardi, F., Barbanti, A., Bastianini, M., Benetazzo, A., Cavaleri, L., Chiggiato, J., Papa, A., Pomaro, A., Sclavo, M., Tosi, L., Umgiesser, G., 2016. The 1966 flooding of Venice – what time taught us for the future. *Oceanography* 29 (4). <https://doi.org/10.5670/oceanog.2016.87>.
- Umgiesser, G., Ferrari, C., Cucco, A., De Pascalis, F., Bellafiore, D., Ghezzi, M., Bajo, M., 2014. Comparative hydrodynamics of 10 Mediterranean lagoons by means of numerical modeling. *J. Geophys. Res. Oceans* 119 (4), 2212–2226.